

**Proximity effects on H absorption in ultrathin V layers**Gunnar K. Pálsson,<sup>1</sup> A. K. Eriksson,<sup>2</sup> M. Amft,<sup>3</sup> X. Xin,<sup>1</sup> A. Liebig,<sup>1,\*</sup> Sveinn Ólafsson,<sup>2</sup> and Björgvin Hjörvarsson<sup>1</sup><sup>1</sup>*Department of Physics and Astronomy, Uppsala University, Box 516, SE-75120 Uppsala, Sweden*<sup>2</sup>*Science Institute, University of Iceland, 107 Reykjavik, Iceland*<sup>3</sup>*Swedish Radiation Safety Authority, Solna Strandväg 96, 171 16 Stockholm*

(Received 2 June 2014; published 22 July 2014)

We discuss proximity effects on the hydrogen uptake in 14 atomic layers of vanadium. The enthalpy and entropy of solution were measured and compared to *ab initio* density functional calculations. We show that there exists a large difference in the hydrogen uptake of V in Cr/V and Fe/V superlattices, in which the V is under close to identical strain states. The calculations show that neither local strain effects nor charge redistributions can be the cause for the observed effect. This leaves magnetic and long ranged elastic strain fields—neither captured by the current calculations—as possible mechanisms for the observed effects.

DOI: [10.1103/PhysRevB.90.045420](https://doi.org/10.1103/PhysRevB.90.045420)

PACS number(s): 61.05.cm, 61.05.cp, 68.55.Ln, 68.65.Cd

**I. INTRODUCTION**

The physical properties of thin films are in many cases strongly affected by the presence of boundaries such as the sample surface, other material layers, and the substrate. This is for example clearly seen in the onset of superconductivity of thin films, which is strongly altered by the thickness of the superconducting layer [1] as well as the composition and the thickness of the neighboring layers. Such proximity effects are not restricted to superconductivity. For example, the magnetic spin-density wave in Cr layers has been shown to be affected by the thickness of the V layers in Cr/V heterostructures [2,3]. Even minute changes in the electronic structure of the V layer were found to have profound effects on the magnetic properties of Cr, which was demonstrated by introducing H into the V layer. H is readily absorbed in the V while absorption is endothermic in Cr. Even small changes of the H concentration in the V resulted in large changes in the spin-density waves of the 50 nm thick Cr layer [4], highlighting the importance of boundaries. The H-induced changes in the electronic structure have also been used to alter the interlayer exchange coupling in magnetic superlattices. The interlayer exchange coupling between the Fe layers in Fe/V superlattices and Fe/Nb multilayers were even observed to change sign when H was introduced in the V (Nb) layers [5–8].

An influence from the nonabsorbing layer on the H uptake of the absorbing layer is also conceivable. Hydrogen uptake of materials depends on the shape and size of the sample [9–11]. This effect of the nonabsorbing layer scales with the size of the absorbing layer, and it is therefore of interest to explore the response in the extreme limit, for example when the absorbing material is only a few monolayers thick. Superlattices offer a unique possibility to explore such effects as they can be grown with good crystal quality and with well defined layer thickness. Due to lattice mismatch between constituents in a superlattice and minimization of the interface free energy, the layers in the superlattice generally become strained. The magnitude and the sign of the strain can be chosen by the selection of the composition and the thickness of the layers, i.e., the

amplitude of the strain can be altered by the thickness ratio of the layers. For example, V is under a biaxial compressive strain in Fe/V [12,13] superlattices while it is under biaxial tensile strain in Mo/V [14]. The different initial strain states of V also affect the electronic structure at the interstitial sites whereby the local binding energy of hydrogen to the host is altered. The binding energy of H in V layers differs therefore significantly in Fe/V and Mo/V superlattices [15,16]. The hydrogen-hydrogen (H-H) interaction also depends on the choice of the nonabsorbing layer. Attractive interaction was observed for H concentrations up to 0.4 [H/V] in Mo/V (001), while the H-H interaction becomes already repulsive at around 0.07 [H/V] in Fe/V (001). The different strain states of V in the two superlattices was inferred to be the major cause of the changes in the absorption potential [15,16].

The influence of the strain state on the H absorption, originating in local electronic changes, is known to be important. Other electronic effects, which do not specifically manifest themselves through changes in lattice constants, are less explored. Close to identical strain states of V are accessible in Fe/V (001) and Cr/V (001) superlattices by appropriate selection of the thickness ratio of the layers. Fe and Cr have close to identical lattice parameters, while Fe has two more valence electrons than Cr and is ferromagnetic in the bulk whereas Cr exhibits antiferromagnetism at room temperature. These material combinations are therefore ideal for exploring electronic proximity effects on the hydrogen uptake in superlattice structures.

**II. EXPERIMENTAL**

Cr/V (001) superlattices were grown on polished single-crystal MgO (001) substrates at 620 K using dc magnetron sputtering. The samples used for the thermodynamic analysis had a thickness of 166 nm with layer sequences [14 ML Cr / 14 ML V]<sub>40</sub>, [7 ML Cr / 14 ML V]<sub>54</sub> where ML stands for monolayer. The subscript denotes the number of repeats of the bilayers. The first layer grown on the substrate was V while the outermost layer of the superlattice was Cr. An additional sample, [6 ML Cr / 22 ML V]<sub>20</sub>, was grown for in-situ x-ray studies of the H induced lattice changes. The samples were covered with 5 nm of palladium to catalyse the H uptake and to prevent oxidation of the samples. X-ray

\*Present address: Institute of Physics, University of Augsburg, D-86135 Augsburg, Germany.

reflectivity (XRR) and high angle x-ray diffraction (XRD) measurements were performed, before and after H loading using a Siemens D-5000 diffractometer in Bragg-Brentano (focusing) geometry, to obtain information about the chemical modulation and the crystalline structure. The mosaicity was determined to be  $0.44^\circ \pm 0.05^\circ$  before and  $0.42^\circ \pm 0.05^\circ$  after repeated H cycling of the Cr/V 7/14 sample and  $0.54^\circ \pm 0.05^\circ$  and  $0.49^\circ \pm 0.05^\circ$  for the Cr/V 14/14 sample. The growth of Cr/V(001) and Fe/V(001) are therefore similar from a structural point of view. More detailed information about the sample growth and structure can be found in Refs. [12] and [17].

The hydrogen uptake was determined using a four point measurement probe (Keithley 199) in an UHV loading system. The pressure was determined using three capacitance pressure gauges with the ranges of 0–10 mbar, 0–100 mbar, and 0–1000 mbar, giving accurate pressure readings over more than six orders of magnitude. The H<sub>2</sub> gas was purified using a NuPure3 gas purifier. The evacuation was performed using a turbomolecular pump, and the composition of the residual gas was determined using a residual gas analyzer (RGA). The base pressure was below  $10^{-8}$  mbar and the dominating residual gas was H<sub>2</sub> gas. Before being exposed to H<sub>2</sub> gas, the sample was heated using a Eurotherm 94C temperature controller with an accuracy of  $\pm 1^\circ\text{C}$ . The temperature was measured directly beneath the sample, giving reliable measurement of the actual temperature. The system was flushed with H gas four times prior to the initiation of the measurements. During the measurement the H<sub>2</sub> gas pressure was increased stepwise, from vacuum to 1 bar while the electrical resistance was measured. The time required to reach equilibrium varied strongly, from a few to more than one thousand minutes, depending on the H concentration, temperature, and pressure used. The temperature ranges used for the pressure-resistance-temperature (prT) measurements of the samples were 473–573 K, 448–548 K, and 433–533 K for the Cr/V 14/14, 7/14, and 6/22 samples, respectively, due to different ranges of stability of the Pd capping layer. The initial H loading/unloading cycle was repeated at each temperature to verify the reversibility.

The relation between the change in resistance and H content was determined using samples without the Pd capping. The Cr/V 7/14 calibration sample was loaded with H at 523 K under a H<sub>2</sub> pressure of 22 mbar, which corresponds to a maximum in the resistance for the Pd capped Cr/V 7/14 sample. The sample was kept under H<sub>2</sub> pressure until the measured resistance had stabilized. At that point the sample was rapidly cooled to room temperature, to ensure conservation of the H content. The  $^1\text{H}(^{15}\text{N}, \alpha\gamma)^{12}\text{C}$  nuclear reaction [18] was then used to determine the H content of the sample. The measurements were performed at the Tandem Accelerator at the University of Uppsala. The average H content in the V layers was determined to be  $\text{VH}_{0.32 \pm 0.02}$  using a  $\text{TaH}_{0.47 \pm 0.01}$  calibration sample [19]. This value is close to the H concentration which has earlier been observed in Mo/V superlattices at the maximum in the resistance [15].

The volume expansion was measured on the Cr/V 6/22 sample using XRR. The measurements were performed in a dedicated Bruker D8, with ultrahigh vacuum in-situ capabilities, in which the sample was exposed to H gas at 513 K. The operating wavelength was  $\lambda = 0.15406$  nm (CuK $\alpha_1$  radiation)

which was selected by a Göbel mirror and a beam compressor yielding a wavelength spread of  $\Delta\lambda/\lambda = 1 \times 10^{-4}$ .

### Theoretical methods

The scalar-relativistic *ab initio* density functional theory (DFT) calculations were performed using the projector augmented wave (PAW) [20,21] method as implemented in VASP [22,23]. The exchange-correlation interaction was treated in the generalized gradient approximation (GGA) in the parametrization of Perdew, Burke, and Ernzerhof (PBE) [24]. A cutoff energy of 400 eV was used and a Gaussian smearing with a width of  $\sigma = 0.05$  eV for the occupation of the electronic levels. For the calculations the  $3d^4$  and  $4s^1$  states of vanadium, the  $3d^5$  and  $4s^1$  states of chromium, as well as the  $3d^7$  and  $4s^1$  states of iron were treated as valence states.

In the experiments the superlattices were grown epitaxially on a magnesium oxide (100) surface, and depending on the layer thicknesses the in-plane strain ranges from 1.3 to 2.6%. The Fe/V and Cr/V superlattices were modeled by repeating a  $1 \times 1 \times N$  ( $2 \times 2 \times N$ ) supercell, with  $N$  ranging from 7 to 10 monolayers (ML) of iron (chromium) and an equal number of vanadium ML's, in the  $z$  direction. We used a constant in-plane strain of 1.6% for all these supercells, i.e., an in-plane lattice constant of 0.293 nm. Note: the calculated bulk lattice constant of V is 0.298 nm. In order to estimate the impact of the strain on the absorption energies, we repeated the 8/8 ML calculations with an in-plane strain of 2.6%, i.e., an in-plane lattice constant of 0.2903 nm. Additionally, we studied two artificial V systems. One under an in-plane strain of 1.6%, which was only allowed to relax in the  $z$  direction. The second system had the bulk V lattice parameters and was allowed to isotropically relax upon H absorption.

A Monkhorst-Pack  $\Gamma$ -centered  $14 \times 14 \times 3$   $k$ -point mesh (296  $k$  points in the irreducible wedge of the Brillouin zone) was used in the  $1 \times 1$  ML supercells and a  $7 \times 7 \times 3$   $k$ -point mesh (74  $k$  points) in the  $2 \times 2$  supercells. The relaxation cycle was stopped when the Hellmann-Feynman forces had become smaller than  $5 \times 10^{-2}$  eV/nm. Spin polarization was not taken into account in the presented calculations.

The charge transfers within the systems have been calculated by means of the Bader analysis [25–27]. Note that the core electrons of the metal atoms have to be taken into account for the Bader analysis [28].

### III. RESULTS AND DISCUSSION

The hydrogen uptake of the samples was determined using resistance measurements, as described above. Representative results are shown in Fig. 1. The measurements were repeated several times for each temperature for both increasing and decreasing applied H pressure. No hystereses were observed during the H loading-unloading cycles. Furthermore, the uptake was close to reversible; the resistance consistently returned to within 2% of its initial value after evacuation. After repeated loading-unloading cycles, the time required for reaching equilibrium increased. This was most prominent at the lowest temperatures, where the time to reach equilibrium was as long as 12 h. The long absorption time was found to be due to the degradation of the Pd-capping layer. X-ray

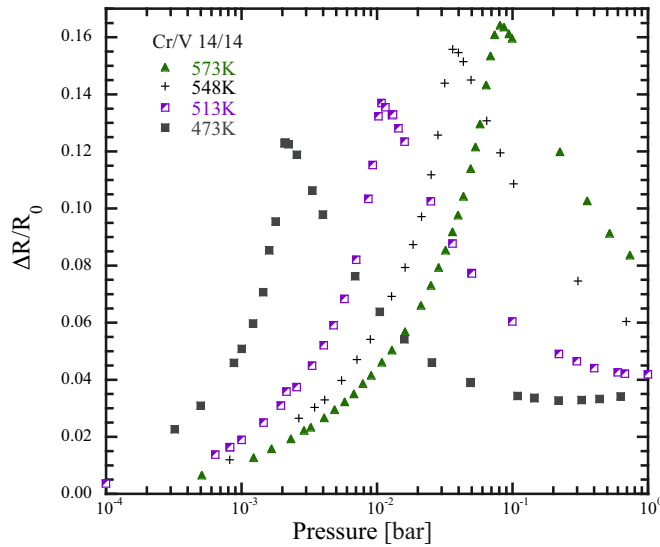


FIG. 1. (Color online) The relative changes in resistance in the Cr/V 14/14 sample as a function of H pressure at different temperatures. The results from Cr/V 7/14 showed the same trend.

reflectivity measurements showed decreased amplitude of the Kiessig fringes from the Pd, consistent with a significant roughening of the layer. Therefore, we redeposited a Pd layer to explore the role of the roughening on the uptake kinetics. The kinetics were restored, confirming the cause of the decrease in uptake rate. Such a degradation has not been observed for Pd layers deposited on V surfaces, highlighting the difference in the adhesion or mixing of Pd on V as compared to Cr.

In Fig. 1, the relative change in resistance  $\Delta R/R_0$  is plotted as a function of applied  $H_2$  pressure. Here,  $R_0$  is defined as the resistance of the H free film measured at 303 K. As seen in the figure, the electrical resistance increases with increasing  $H_2$  pressure, until a maximum is reached ( $\Delta R_{\max}$ ). Thereafter it decreases and at the lowest temperature a shallow local minimum ( $\Delta R_{\min}$ ) is observed. This response in the electrical resistance as a function of applied H pressure has been observed earlier in thin V films [29,30] and in Mo/V superlattices [15]. In Fe/V, the resistance increases monotonically up to a [H/V] ratio close to 1 [31,32]. A clear increase in  $\Delta R_{\max}$  is observed with increasing temperature, similar to the changes observed in thin V films [29,30]. In Mo/V superlattices the temperature dependence is the opposite:  $\Delta R_{\max}$  decreases with increasing temperature while  $\Delta R_{\min}$  is independent of temperature in Fe/V superlattices [31]. These differences are currently not understood.

The change in resistance can be used to determine the average H concentration ( $\langle c \rangle$ ) as described in Ref. [15]:

$$\frac{\Delta R(c)}{R_0} = \frac{\Delta \rho(c)}{\rho_0} \approx a(c) + b(c)^2. \quad (1)$$

The constants,  $a$  and  $b$ , can be calculated by determining the H concentration in the V layers and the obtained change in resistance at the extreme point(s). Here the H concentration at  $\Delta R_{\max}$  in the Cr/V superlattice was determined using  $H^1(N^{15}, \alpha\gamma)C^{12}$  nuclear reaction analysis, as described above. The scaling between resistance and concentration holds well at temperatures above the transition temperature, but fails below.

The transition temperature was estimated using Curie-Weiss analysis for both samples, defining the range of the validity of the concentration determination, as discussed below.

Recently, however, it has been pointed out that resistivity is sensitive to fluctuations in the hydrogen density, even above the ordering temperature [33]. To test the influence of this we measured the optical transmission through the 14/14 Cr/V superlattice and the resistivity simultaneously as a function of applied hydrogen pressure and temperature. The enthalpies extracted from resistivity converted to concentration, and the enthalpies determined from converting optical transmission to concentration showed only minor differences within the relevant temperature interval. Thus we only show the enthalpy and entropy as determined from resistivity.

A hydrogen depleted interface region ( $\Delta$ ) is observed in both Fe/V and Mo/V superlattices, which can extend to 3 ML at low H concentrations [16,34,35]. The average concentration ( $\langle c \rangle$ ) is therefore lower than the concentration in the interior region of the layers ( $c_{\text{in}}$ ). The relation between  $c_{\text{in}}$  and  $\langle c \rangle$  is easily determined when  $\Delta$  is known by

$$c_{\text{in}} = \langle c \rangle \frac{L_V}{(L_V - 2\Delta)}, \quad (2)$$

where  $L_V$  denotes the thickness of the V layers.  $\Delta$  is not known for Cr/V superlattices and therefore all concentrations presented here are the average H concentrations in the V layers.

The determined H concentration as a function of pressure and temperature is illustrated in Fig. 2 for one of the samples. The isotherms are shown up to 0.32 [H/V], which is close to the upper limit for the unique determination of the H concentration. The transition temperatures were determined to be  $500 \pm 5$  K,  $463 \pm 2$  K, and  $480 \pm 10$  K for the Cr/V 14/14, Cr/V 7/14, and Cr/V 6/22 samples, respectively, using the changes in the inflection points in the pressure-concentration-temperature (pcT) diagrams. All the thermodynamic analyses were restricted to temperatures above these temperatures. As a comparison, the critical temperature was determined to be

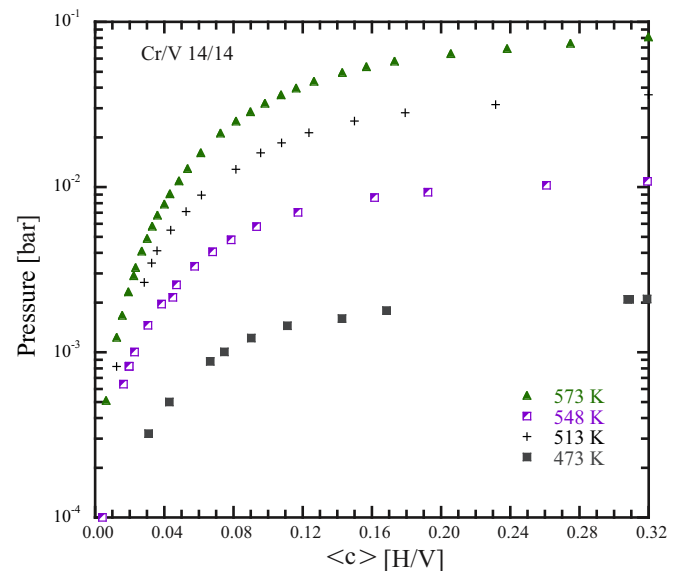


FIG. 2. (Color online) Pressure composition isotherms for Cr/V 14/14.

460 ± 20 K in thin V (001) films [30]. The isotherms were used to evaluate the enthalpy ( $\Delta\bar{H}_H$ ) and entropy ( $\Delta\bar{S}_H$ ) of solution, using the Van't Hoff relation

$$\Delta\mu_H = \frac{1}{2}k_B T \ln\left(\frac{p}{p_0}\right) = \Delta\bar{H}_H - T\Delta\bar{S}_H, \quad (3)$$

where  $p$  is the H pressure,  $p_0$  is the reference pressure,  $T$  is the absolute temperature, and  $k_B$  is the Boltzmann constant.

The deduced enthalpy of solution is shown in Fig. 3, where we also include the previously published results for bulk V [36] and representative results for Fe/V 3/10 and Fe/V 14/14 superlattices. The average H concentrations in the Fe/V superlattices, presented in Fig. 3, were calculated using Eq. (2). The binding energy is less negative (weaker) for Cr/V 14/14, as compared to the bulk  $\alpha$  phase at low, i.e., < 0.08, [H/V]. Large changes are observed in the results from the Cr/V 7/14 sample, in which the binding energy is more negative (stronger) than in bulk  $\alpha$  phase. The enthalpy in the infinite dilution limit was obtained by extrapolation to [H/V] = 0, and the results are shown in Table I.

The result from the Cr/V 14/14 samples is close to what is observed in the Fe/V superlattices ( $-0.15 \pm 0.02$  eV/H) for the same strain state. Sievert analyses were also performed, and the results were in excellent agreement with the results from the Van't Hoff analysis.

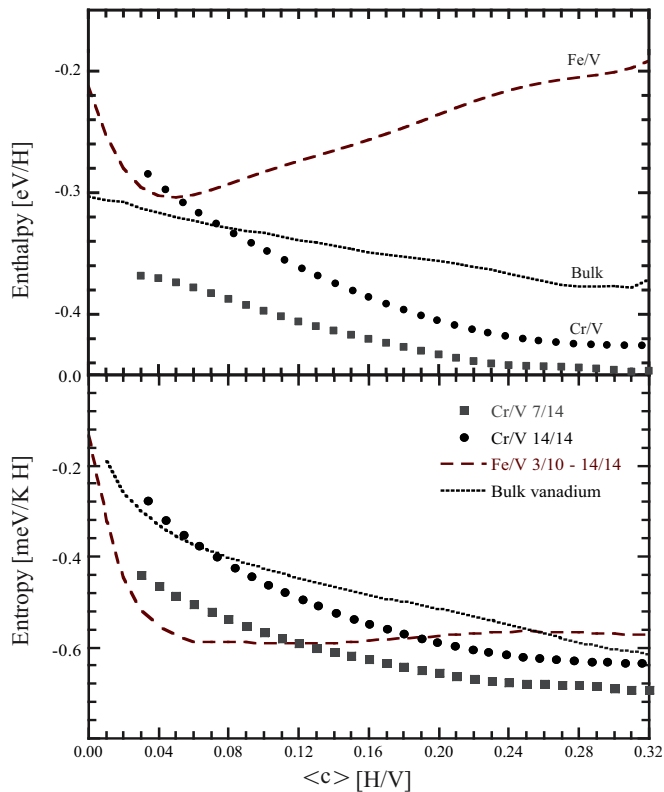


FIG. 3. (Color online) The enthalpy  $\Delta\bar{H}$  (upper panel) and entropy of solution  $\Delta\bar{S}$  (lower panel) as a function of H concentration for the Cr/V 14/14 and 7/14 superlattices. The results for the V bulk  $\alpha$  phase are from Ref. [36]. The results for the Fe/V samples are representative for Fe/V 14/14 and Fe/V 3/10 superlattices. The data is taken from Ref. [31]. The uncertainty is less than 0.07 eV/H for the enthalpy and 0.01 meV/KH for the enthalpy.

TABLE I. Enthalpy of solution at infinite dilution and at 0.32 [H/V] for Cr/V, Fe/V 14/14 [31] bulk V [36] along with the hydrogen-hydrogen interaction at low H concentrations. The uncertainties are less than 0.02 eV/H for all experimental results presented in the table. For comparison the calculated enthalpies from the 8/8 Cr/V and Fe/V superlattices, as well as two artificial V systems, are shown.

Sample:	$\Delta\bar{H}^0$ [eV/H]	Experiment	
		$\Delta\bar{H}(c = 0.32 [H/V])$ [eV/H]	H-H [eV/H]
Cr/V 7/14	-0.36	-0.45	-0.39
Cr/V 14/14	-0.22	-0.43	-1.14
Fe/V 14/14	-0.15	-0.22	-2.75
Bulk V	-0.30	-0.40	-0.33
Calculations			
Structure:	$\Delta\bar{H}^0(c = 0.03 [H/V])$	$\Delta\bar{H}(c = 0.25 [H/V])$	H-H
Cr/V 8/8	-0.295 <sup>a</sup>	-0.335 <sup>b</sup>	
Fe/V 8/8	-0.277 <sup>a</sup>	-0.334 <sup>b</sup>	
V 8 <sup>c</sup>	-0.264 <sup>a</sup>	-0.318 <sup>b</sup>	
V bulk <sup>d</sup>	-0.318 <sup>a</sup>	-0.194 <sup>b</sup>	
Cr/V 8/8	-0.257 <sup>e</sup>	-0.351 <sup>f</sup>	
Fe/V 8/8	-0.201 <sup>e</sup>	-0.349 <sup>f</sup>	

<sup>a</sup>distorted tetrahedral, 1.6% in-plane strain

<sup>b</sup>octahedral, 1.6% in-plane strain

<sup>c</sup>An 8 ML thick V supercell under 1.6% in-plane strain, where H was absorbed at the same sites as in the 8/8 superlattices.

<sup>d</sup>An 8 ML thick V supercell with bulk lattice parameters that was allowed to isotropically expand. H was absorbed at the same sites as in the 8/8 superlattices.

<sup>e</sup>distorted tetrahedral, 2.6% in-plane strain

<sup>f</sup>octahedral, 2.6% in-plane strain

To explore the possible proximity effects on the H-binding energy, let us now compare the results from Cr/V(001) and Fe/V(001) superlattices. Fe and Cr form bcc structures with similar lattice constants,  $a_{Fe} = 0.286$  nm and  $a_{Cr} = 0.291$  nm, respectively, while the lattice parameter of V is 0.303 nm. The strain  $\epsilon_{xx}$  was calculated using

$$\epsilon_{xx} = \frac{\Delta a}{a_0}, \quad (4)$$

where  $\Delta a$  is the change in the in-plane lattice parameter and was found to be  $\epsilon_{xx} = -2.4\%$  in Cr/V 14/14 and  $\epsilon_{xx} = -2.0\%$  in Cr/V 7/14. The compressive strain in Cr/V 6/22 is  $\epsilon_{xx} = -1.3\%$ . This strain state lies in between the strain states obtained for the Fe/V 3/10 and 14/14 ( $\epsilon_{xx} = -1.3\%$  and  $\epsilon_{xx} = -2.6\%$ , respectively) [32]. Superlattices of Fe/V and Cr/V, with similar layer thicknesses, are therefore expected to give rise to a similar biaxial compressive strain in the V layers. The initial biaxial compressive strain gives rise to a decrease in the lattice volume of V due to Poisson lattice response. The interstitial electron density, governed by the lattice volume, is thereby increased. The binding energy of H is expected to reflect these differences at the lowest concentrations.

Let us now consider the H-H interaction energies at low concentrations. The strength can be determined using

$$\Delta\bar{H} = \Delta\bar{H}^0 + c\bar{u}_{HH}, \quad (5)$$

where  $\Delta\bar{H}^0$  is the binding energy in the infinite dilution limit and  $\bar{u}_{HH}$  is the total effective H-H interaction [37] (measured

by the slope of the curves in Fig. 3). The strength  $\bar{u}_{\text{HH}}$  in the Cr/V superlattices is larger than in the bulk  $\alpha$  phase of V. At low H concentrations  $\bar{u}_{\text{HH}}$  is much stronger in Cr/V 14/14 than in the Cr/V 7/14. The strength decreases with increasing H concentration. That  $\bar{u}_{\text{HH}}$  increases with increasing biaxial strain state is in agreement with earlier observations for V (001) [38]. The observed changes in  $\bar{u}_{\text{HH}}$  are therefore in qualitative agreement with the observed changes in the transition temperature.

At concentrations below 0.07, an attractive H-H interaction is observed in Fe/V(001) (negative slope), see Fig. 3. This attractive interaction is approximately the same in both the Fe/V samples, twice what is found for the Cr/V 14/14 sample and about six times larger than in the Cr/V 7/14 sample, see Table I. At higher H concentrations,  $\bar{u}_{\text{HH}}$  becomes repulsive in the Fe/V superlattices. A repulsive H-H interaction has also been observed in biaxially compressed thin layers of Nb in W/Nb superlattices in contrast to what is found for the Cr/V samples in the concentration interval investigated [38]. The H binding energy levels off and reaches a more negative value in Cr/V 7/14 as compared to bulk  $\beta$  phase V ( $-0.40 \pm 0.03$  eV/H) [39]. For the Cr/V 14/14 sample, the enthalpy levels off at  $-0.43 \pm 0.01$  eV/H. The differences in the absorption are therefore large between V layers in Fe/V and Cr/V (001) superlattices. The V layers are under a similar biaxial strain state in these structures, and the difference must therefore be ascribed to proximity effects other than strain.

The change in entropy is displayed in the lower panel in Fig. 3 along with the entropy change in the bulk V  $\alpha$  phase and a line representing the results from the Fe/V 3/10 and 14/14 samples [31]. Within the uncertainty of the measurements, the Cr/V 14/14 sample exhibits similar trends to the bulk phase at low H concentrations. The change in entropy decreases (less negative) with increasing strain over all the concentration range investigated here.

We approximate the enthalpy of solution of  $n$  hydrogen atoms in the unit cell of the superlattice M/V by the change in the total electronic energy  $U$

$$\Delta\bar{H} \approx \Delta U = \frac{1}{n} \left[ U(\text{M}/\text{VH}_n) - U(\text{M}/\text{V}) - \frac{n}{2} U(\text{H}_2) \right], \quad (6)$$

thus neglecting other contributions, for instance from the zero point energy and temperature. For a number of hydrides these contributions have been shown to account for  $-0.1$  eV on average, i.e., a rather constant overestimation of  $\Delta\bar{H}$  when approximated by  $\Delta U$  [40].

The enthalpy was calculated for hydrogen occupying either the tetrahedral or octahedral  $z$  sites in Fe/V and Cr/V superlattices, and the results are summarized in Fig. 5. It is important to point out that the hydrogen was initially inserted into the tetrahedral site. During the structural relaxation of the lower concentration systems, it relaxed into so-called distorted tetrahedral sites with coordinates  $(0, u < 0.25, z)$ . Figure 4 shows the octahedral (a), distorted tetrahedral (b), and tetrahedral (c) sites. For higher concentrations, i.e.,  $c > 0.2$ , the H relaxed from the initial tetrahedral sites into the octahedral sites. Hence the enthalpies coincide with those obtained from calculations with H initially in the octahedral sites, see Fig. 5.

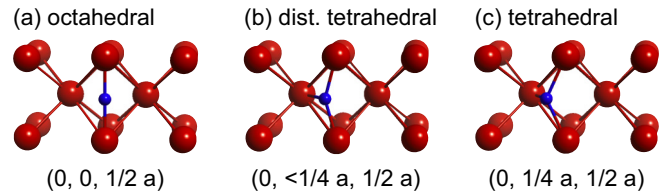


FIG. 4. (Color online) Hydrogen situated at different interstitial sites in the vanadium lattice. The vanadium atoms are depicted by red spheres and the hydrogen atom by a smaller blue sphere. Panel (a) shows hydrogen sitting into an octahedral  $z$  site, panel (b) shows hydrogen sitting at a slightly distorted tetrahedral position, and finally (c) depicts hydrogen absorbed onto a tetrahedral site. The distorted site is found by the calculations to be a stable configuration.

The overall magnitude of the calculated enthalpy change is in good agreement with the experiments for low H concentrations, highlighting the appropriateness of the approximations in this limit. However, at higher H concentrations, i.e., above 0.05 [H/V], the Cr/V and Fe/V system showed opposite behaviors in the experiments: While the H-H interaction in Cr/V becomes more attractive with increasing concentration, it becomes more repulsive in the case of Fe/V. The calculations do not reproduce this behavior at higher H concentrations, Fig. 5, as there is overall very little difference between the calculated enthalpies of Cr/V and Fe/V. The reason lies in the close similarity of the V layers in both calculated structures. First, their in-plane strain is identical and the out-of-plane expansion is only 4% larger in Cr/V than in Fe/V. Second, the H atoms are expected to absorb in the middle of the V layers [35]. Their absorption enthalpies are predominantly determined by the structure of the metal lattice in their proximity, which is very similar in the Cr/V and Fe/V system. Figure 6 shows the partial density of states (pDOS) of V atoms at the Cr/V (Fe/V) interface (top panels) and in the middle of the V layer (bottom panels). Note the great similarity in the pDOS of the V atoms in the middle layers of Cr/V and

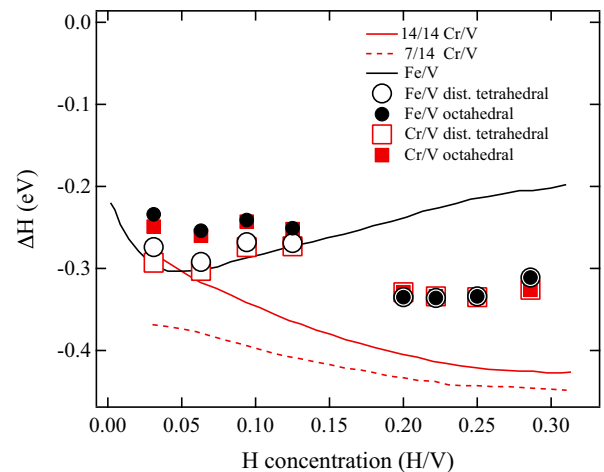


FIG. 5. (Color online) Calculated absorption enthalpies of H in Fe/V (circles) and Cr/V (squares) in comparison to experimentally obtained enthalpies of solution (lines) from Fig. 2. Note that at lower H concentrations the distorted tetrahedral sites are favored, while at higher concentrations also initial tetrahedral H positions relax into the octahedral sites.

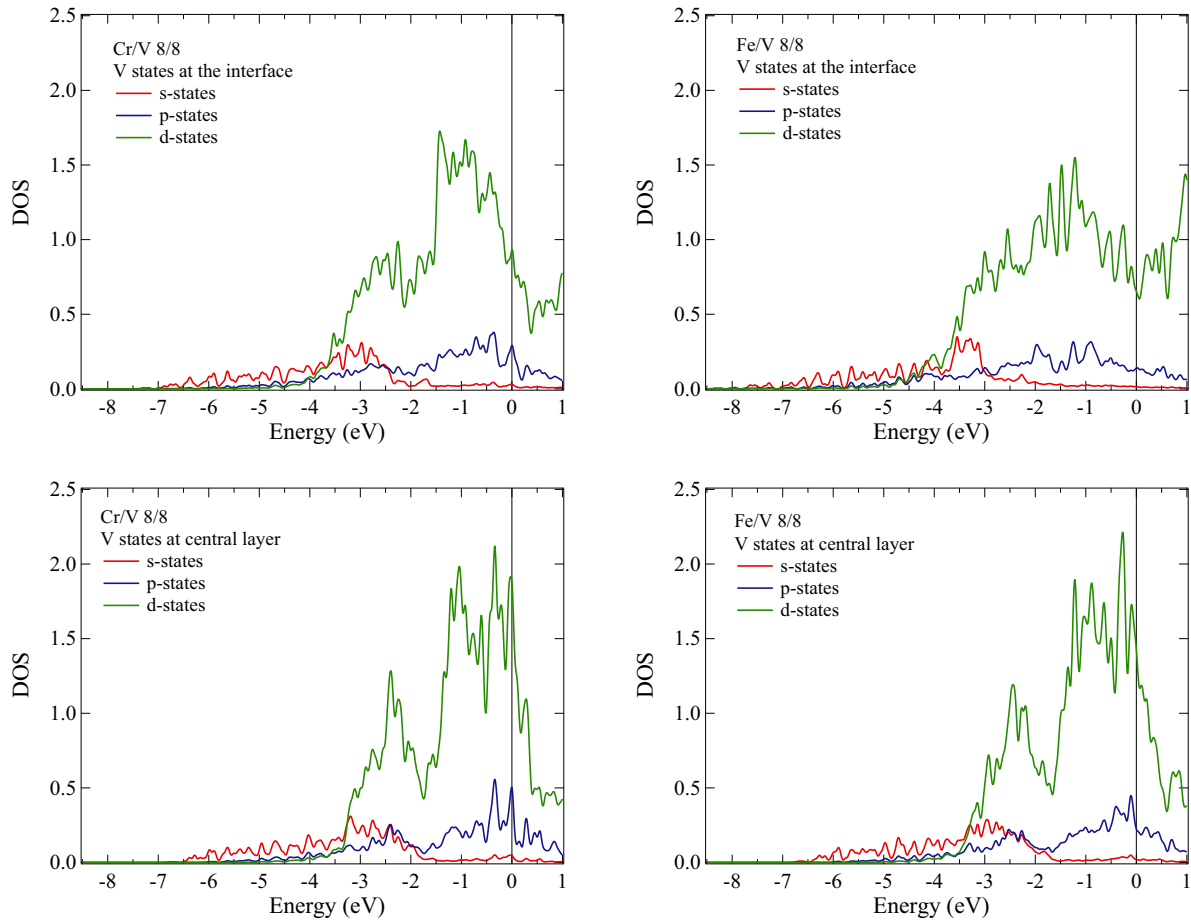


FIG. 6. (Color online) Partial density of states of V atoms at the Cr/V (Fe/V) interface (top panels) and in the middle of the V layer (bottom panels). Note the great similarity in the latter case. At the interface charge is transferred from the V  $d$  states into the Cr (Fe)  $d$  states.

Fe/V, which determine the local chemical environment of the absorbed H atoms, cf. Fig. 6.

At the V-Cr(Fe) interface the V atoms donate  $0.2 e^-$  ( $0.4 e^-$ ) from their  $d$  states into the neighboring Cr (Fe)  $d$  states. This charge redistribution is essentially restricted to the single atomic layers at the interface. Hence the center of the metal layers is unaffected by this interface charge redistribution.

In Fig. 7 we show the sum of the pDOS of the H atom, absorbed at the distorted tetrahedral site for a concentration of  $1/32$ , and its four nearest-neighbor V atoms. In addition to the  $8/8$  Cr/V and Fe/V systems (Fig. 7, top panels), we also studied two artificial systems to distinguish structural effects from electronic effects induced by the presence of the Fe/Cr layers (Fig. 7, bottom panels). In all four studied systems the chemical binding of H in the V lattice is dominated by the hybridization of H  $s$  states and V states at approximately  $-7.2$  eV. This is in agreement with previous calculations as well as experiment [41,42]. These states are indistinguishable in the strained V and the Cr/V (Fe/V) systems, while they are slightly shifted towards higher energies in the bulk V system. Differences in the lattice parameters and the different metals in the superlattice, i.e., Cr and Fe, affect mostly the  $p$  and  $d$  bands above  $-4$  eV and not the chemical binding of H.

Bader analysis of the four studied systems shows that a net charge of  $-0.60$  to  $-0.62 e^-$  is transferred to the absorbed H

atom in these systems, which is in agreement with calculations by About [28]. This value is larger and of the opposite sign than previously estimated as a result of an x-ray spectroscopic study by Duda *et al.* which gave  $1/4 e^-$  (Ref. [43]) donated to the  $3d$  band of V as a result of hydrogen absorption. This result was however not obtained using rigorous Bader analysis. The fact that charge is seen to accumulate around the H is consistent with the higher electronegativity of hydrogen (2.2) compared to V (1.63). Since these charge redistributions are local, the influence of Fe and Cr was negligible. At higher H concentrations, i.e., 25%, we found the same net charge transfer to H. Still, the increased Coulomb repulsion of the H atoms did not result in a decrease of the absorption enthalpies, as seen in Fig. 5. An increase of the in-plane strain from 1.6 to 2.6% did not alter the obtained charge transfer.

Absorbing H in the strained superlattices causes a volume expansion. Due to the in-plane strain this expansion can only occur in the  $z$  direction, i.e., the  $c/a$  ratio increases. Here the V embedded in Cr and Fe layers behave differently. While the total expansion in the  $z$  direction of the multilayer is almost identical for both systems (0.4 and 0.3%, respectively) the expansion of the V layer upon H absorption at the distorted tetrahedral sites varies significantly between the systems (2.9 and 5%, respectively, for 1.6% in-plane strain). Hence the Fe layer compensates more for the V expansion than the Cr layer.

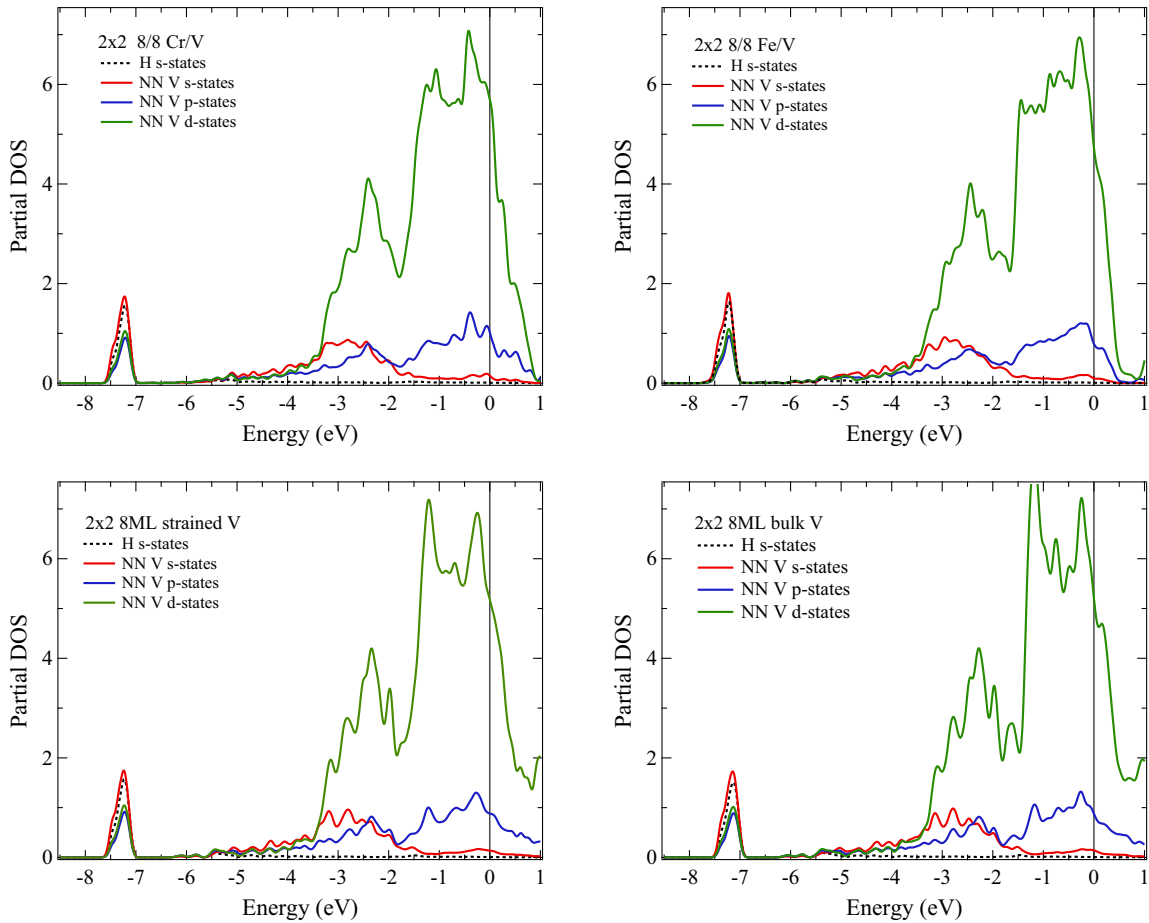


FIG. 7. (Color online) Partial density of states of H at the tetrahedral site and the four nearest-neighbor V atoms in bulk V (top left), strained V (top right), Cr/V (bottom left), and Fe/V (bottom right). The chemical binding of H in the V lattice is dominated by the hybridization of H and V states at approx.  $-7.2$  eV. These states are indistinguishable in the strained V, Cr/V, and Fe/V system, while they are slightly shifted towards higher energies in the bulk V system.

In case of 2.6% in-plane strain the effect is less pronounced, i.e., 0.5 and 1.5% for Cr and Fe only. The large initial distortion in the  $z$  direction is most likely the reason for this behavior.

In Table II the H lattice parameter  $u$  is shown for four distorted tetrahedral absorption sites, cf. Fig. 6. While  $u = 0.25$  at the ideal tetrahedral site, it changes from 0.082 to 0.182 in the studied model systems. Therefore we call these absorption sites distorted tetrahedral sites.

The distortion is more pronounced, i.e.,  $u$  is smaller, for superlattices with a larger initial in-plane strain. This rationalizes the calculated absorption energies at low H concentrations, as shown in Table I. The exceptional small enthalpy in Fe/V in the 2.6% strain state is more similar to the absorption at the octahedral site, which was shown in Fig. 5 to be energetically less favorable than the distorted tetrahedral site.

TABLE II. Calculated lattice position  $u$  of H absorbed at the distorted tetrahedral site, 0.25 at the ideal tetrahedral site.

	$u$ (1.6% strain)	$u$ (2.6% strain)
$2 \times 2$ 8/8 Cr/V	0.182	0.130
$2 \times 2$ 8/8 Fe/V	0.176	0.082

From these results we can conclude that the strain state of the V layer has a larger impact on the H absorption than the choice of the second metal in the superlattice. However, the local effects that have been taken into account here are not sufficient to explain the observed differences in the H absorbed in Fe/V and Cr/V, and we call for further theoretical studies of these systems. A number of physical properties and effects, respectively, that have been neglected in this study can be pointed out. First, spin polarization was not included in the calculations and thus magnetic effects from the Fe layer can not be excluded, since our nonmagnetic electronic contributions to the total energy difference are not responsible for the observed differences. Second, zero-point energies of H in the V layers might be affected differently by the Fe and the Cr layer. Third, long-range elastic interactions of the H atoms are not accounted for.

#### Lattice expansion

As discussed above, the H induced volume changes are strongly linked to the thermodynamic properties of the absorption. The volume expansion of Cr/V superlattices  $\Delta V/V = k\langle c \rangle$  were therefore determined as a function of concentration at 513 K using x-ray reflectivity. X-ray

reflectivity is insensitive to any local atomic distortions and is therefore a reliable method for determining the global volume changes [44]. The temperature was chosen to ensure that expansion was measured in a single phase, above the phase boundary of the ordered state. The concentration was obtained from the simultaneously measured resistance over the sample. The Cr/V 6/22 results yielded an expansion coefficient of  $k = 0.12 \pm 0.02$ . This value is close to expansion coefficients measured for MoV/V superlattices at low concentrations 0.11(1) [45]. Both of these results are markedly different compared to values obtained from FeV/V 6/21 superlattices, using neutron reflectivity [46] where the expansion coefficient was found to be 0.21(2). All three results can be reconciled using linear elasticity theory and proper handling of clamping effects [47]. Calculating the expansion coefficient using this theory and assuming the dipole force components of the bulk yields 0.12–0.13 for tetrahedral occupancy and 0.19 for octahedral  $z$  occupancy. A reasonable conclusion from this analysis is that hydrogen occupies different sites for Fe/V and Cr/V based superlattices even in the presence of similar strain states. The expansion coefficients were evaluated with DFT and no clear trends could be observed. This is not unexpected since the forces acting on the V atoms due to hydrogen, that give rise to the expansion, are known to not be in agreement with experimental values of the dipole force components [47]. This is probably due to inaccurate potentials for vanadium, which can also be seen by the disagreement of the elastic constants with experiment under applied pressure [48].

We conclude from the volume expansion measurements that due to proximity to Fe hydrogen switches occupancy from tetrahedral to octahedral even at the lowest concentrations. Previous interpretations of the reason for octahedral occupancy in Fe/V superlattices were based on opening up of the octahedral sites due to compressive in-plane strain. If present, this effect cannot be the only reason for a change of site as the experimental data shows. This proximity effect is not present at the level of theory presented here and may be related to

an intricate interplay between hydrogen and magnetic effects in Fe or long-range elastic interactions that also have been neglected in this study. As mentioned above the effect of spin polarization (magnetism) might also occur via the larger lattice constant of real bulk Fe compared to our nonmagnetic Fe. So it might be hard, even with proper spin polarized calculations at hand, to distinguish between the two effects.

#### IV. CONCLUSIONS

Large differences are observed in the H uptake of V in Cr/V and Fe/V (001) superlattices. A difference of 0.2 eV/H was seen in the enthalpy change in V layers having proximity to Cr or Fe layers. The V layers are under similar biaxial compressive strain which eliminates the strain as a cause for the observed differences. A change of site from octahedral to tetrahedral when changing the nonabsorbing layer from Fe to Cr is suggested by elasticity theory and the experimental expansion coefficients. By using *ab initio* density functional theory the nonmagnetic contribution to a proximity effect, i.e., changes in overlap between hydrogen 1s and V 3d orbitals, being the cause for a change of site is excluded since all model systems look locally essentially the same to H. Future work will focus on examining the effect of spin polarization on the hydrogen binding energy and improving the treatment of long-range H-H interactions in the calculations. This surprising result calls for a thorough theoretical exploration of H absorption in strongly confined materials.

#### ACKNOWLEDGMENTS

The work was supported by the Icelandic Research Fund, the Icelandic Scientific Instruments Fund, the Nordic Center of Excellence on Hydrogen Storage Materials, and the Knut and Alice Wallenberg foundation. M.A. is grateful to the Swedish National Infrastructure for Computing (SNIC) for the granted computer time.

- 
- [1] N. R. Werthamer, *Phys. Rev.* **132**, 2440 (1963).
  - [2] E. Kravtsov, A. Nefedov, F. Radu, A. Remhof, H. Zabel, R. Brucas, B. Hjörvarsson, A. Hoser, and S. B. Wilkins, *Phys. Rev. B* **70**, 054425 (2004).
  - [3] E. Kravtsov, R. Brucas, B. Hjörvarsson, A. Hoser, G. McIntyre, A. Nefedov, F. Radu, A. Remhof, and H. Zabel, *J. Magn. Magn. Mater.* **286**, 425 (2005).
  - [4] E. Kravtsov, A. Nefedov, G. Nowak, K. Zhernenkov, H. Zabel, B. Hjörvarsson, A. Liebig, A. Hoser, G. J. McIntyre, L. Paolasini, and A. Remhof, *J. Phys.: Condens. Matter* **21**, 336004 (2009).
  - [5] B. Hjörvarsson, J. A. Dura, P. Isberg, T. Watanabe, T. J. Udovic, G. Andersson, and C. F. Majkrzak, *Phys. Rev. Lett.* **79**, 901 (1997).
  - [6] A. Remhof, G. Nowak, H. Zabel, M. Björk, M. Pärnaste, B. Hjörvarsson, and V. Uzdin, *EPL* **79**, 37003 (2007).
  - [7] F. Klöse, C. Rehm, D. Nagengast, H. Maletta, and A. Weidinger, *Phys. Rev. Lett.* **78**, 1150 (1997).
  - [8] A. Weidinger, D. Nagengast, C. Rehm, F. Klöse, and B. Pietzak, *Thin Solid Films* **275**, 48 (1996).
  - [9] P. F. Miceli and H. Zabel, *Phys. Rev. Lett.* **59**, 1224 (1987).
  - [10] P. F. Miceli and H. Zabel, *Z. Phys. B* **74**, 457 (1989).
  - [11] E. Johansson, C. Chacon, C. Zlotea, Y. Andersson, and B. Hjörvarsson, *J. Phys.: Condens. Matter* **16**, 7649 (2004).
  - [12] P. Isberg, B. Hjörvarsson, R. Wäppling, E. B. Svedberg, and L. Hultman, *Vacuum* **48**, 483 (1997).
  - [13] G. Andersson, B. Hjörvarsson, and H. Zabel, *Phys. Rev. B* **55**, 15905 (1997).
  - [14] F. Stillesjö, B. Hjörvarsson, and H. Zabel, *Phys. Rev. B* **54**, 3079 (1996).
  - [15] F. Stillesjö, S. Olafsson, P. Isberg, and B. Hjörvarsson, *J. Phys.: Condens. Matter* **7**, 8139 (1995).
  - [16] G. Andersson, B. Hjörvarsson, and P. Isberg, *Phys. Rev. B* **55**, 1774 (1997).
  - [17] A. Liebig, G. Andersson, J. Birch, and B. Hjörvarsson, *Thin Solid Films* **516**, 8468 (2008).

- [18] W. A. Lanford, H. P. Trautvetter, J. F. Ziegler, and J. Keller, *Appl. Phys. Lett.* **28**, 566 (1967).
- [19] B. Hjörvarsson, J. Rydén, T. Ericsson, and E. Karlsson, *Nucl. Instrum. Methods Phys. Res. B* **42**, 257 (1989).
- [20] P. E. Blöchl, *Phys. Rev. B* **50**, 17953 (1994).
- [21] G. Kresse and D. Joubert, *Phys. Rev. B* **59**, 1758 (1999).
- [22] G. Kresse and J. Fürthmüller, *Comput. Mater. Sci.* **6**, 15 (1996).
- [23] G. Kresse and J. Fürthmüller, *Phys. Rev. B* **54**, 11169 (1996).
- [24] J. P. Perdew, K. Burke, and M. Ernzerhof, *Phys. Rev. Lett.* **77**, 3865 (1996).
- [25] G. Henkelman, A. Arnaldsson, and H. Jonsson, *Comput. Mater. Sci.* **36**, 354 (2006).
- [26] E. Sanville, S. D. Kenny, R. Smith, and G. Henkelman, *J. Comp. Chem.* **28**, 899 (2007).
- [27] W. Tang, E. Sanville, and G. Henkelman, *J. Phys. Condens. Matter* **21**, 084204 (2009).
- [28] S. Aboud and J. Wilcox, *J. Chem. Phys. C* **114**, 10978 (2010).
- [29] G. Andersson, K. Aits, and B. Hjörvarsson, *J. Alloys Comp.* **334**, 14 (2002).
- [30] J. Bloch, B. Hjörvarsson, S. Olsson, and R. Brukas, *Phys. Rev. B* **75**, 165418 (2007).
- [31] G. Andersson, P. H. Andersson, and B. Hjörvarsson, *J. Phys.: Condens. Matter* **11**, 6669 (1999).
- [32] S. Olsson, P. Blomquist, and B. Hjörvarsson, *J. Phys.: Condens. Matter* **13**, 1685 (2001).
- [33] J. Prinz, G. K. Pálsson, P. T. Korelis, and B. Hjörvarsson, *Appl. Phys. Lett.* **97**, 251910 (2010).
- [34] B. Hjörvarsson, J. Rydén, E. Karlsson, J. Birch, and J. E. Sundgren, *Phys. Rev. B* **43**, 6440 (1991).
- [35] V. Meded and S. Mirbt, *Phys. Rev. B* **71**, 024207 (2005).
- [36] E. Veleckis and R. K. Edwards, *J. Phys. Chem.* **73**, 683 (1969).
- [37] Y. Fukai, *The Metal-Hydrogen System; Basic bulk properties* (Springer, Berlin, Heidelberg, 1993), p. 14.
- [38] S. Olsson, B. Hjörvarsson, E. B. Svedberg, and K. Umezawa, *Phys. Rev. B* **66**, 155433 (2002).
- [39] K. Papathanassopoulos and H. Wenzl, *J. Phys. F: Met. Phys.* **12**, 1369 (1982).
- [40] S. V. Alapati, K. J. Johnson, and D. S. Sholl, *Phys. Chem. Chem. Phys.* **9**, 1438 (2007).
- [41] Y. Fukai, S. Kazama, K. Tanaka, and M. Matsumoto, *Solid State Commun.* **19**, 507 (1976).
- [42] P. H. Andersson, L. Fast, L. Nordström, B. Johansson, and O. Eriksson, *Phys. Rev. B* **58**, 5230 (1998).
- [43] L. C. Duda, P. Isberg, P. H. Andersson, P. Skytt, B. Hjörvarsson, J. H. Guo, C. Sathe, and J. Nordgren, *Phys. Rev. B* **55**, 12914 (1997).
- [44] G. K. Pálsson, A. R. Rennie, and B. Hjörvarsson, *Phys. Rev. B* **78**, 104118 (2008).
- [45] V. Leiner, H. Zabel, J. Birch, and B. Hjörvarsson, *Phys. Rev. B* **66**, 235413 (2002).
- [46] G. K. Pálsson, V. Kapaklis, J. A. Dura, J. Jacob, S. Jayanetti, A. R. Rennie, and B. Hjörvarsson, *Phys. Rev. B* **82**, 245424 (2010).
- [47] G. K. Pálsson, M. Wälde, M. Amft, Y. Wu, M. Ahlberg, M. Wolff, A. Pundt, and B. Hjörvarsson, *Phys. Rev. B* **85**, 195407 (2012).
- [48] L. Koci, Y. Ma, A. R. Oganov, P. Souvatzis, and R. Ahuja, *Phys. Rev. B* **77**, 214101 (2008).